Requirement of An Allosteric Kinetics of NMDA Receptors for
Spike-Timing-Dependent Plasticity

Hidetoshi Urakubo, Minoru Honda, Robert C Froemke, and Shinya Kuroda

Journal of Neuroscience (2008)

# Supplementary Information

**Contents**

Preface ..... 2
Part A: Modeling of Postsynaptic Membrane Potential (Figure 1A) ..... 3
1. Postsynaptic Neuron ..... 3
1.1 Spike-Generating $Na^+$ Current $I_{Na}$ ..... 4
1.2 Delayed-Rectifier $K^+$ Current $I_{DR\text{-}K}$ ..... 4
1.3 A-Type $K^+$ Current $I_{A\text{-}K}$ ..... 5
1.4 L-type Voltage-Gated $Ca^{2+}$ Channel $I_{L\text{-}Ca}$ ..... 6
2. Pre- and Postsynaptic Stimulation ..... 6
2.1 Neurotransmitter Release by Presynaptic Stimulation ..... 6
2.2 Response of Postsynaptic Receptors and the Allosteric Kinetics of NMDARs ..... 7
2.3 Postsynaptic Stimulation ..... 9
Part B: Modeling of Postsynaptic Signaling Cascades (Figure 1B) ..... 10
3. $Ca^{2+}$ Influx and Removal ..... 10
3.1 $Ca^{2+}$ Influx via NMDARs ..... 10
3.2 $Ca^{2+}$ Influx via VGCCs ..... 11
3.3 $Ca^{2+}$ Removal ..... 11
4. Intracellular Signaling Cascades ..... 12
4.1 Formalization of Molecular Interaction ..... 13
4.2 Formalization of Molecular Diffusion ..... 13
4.3 Overview of Molecular Interactions ..... 14
4.3.1 $Ca^{2+}$·CaM Interaction ..... 14
4.3.2 $Ca^{2+}$·CaM·CaMKII System ..... 14
4.3.3 CaN System ..... 15
4.3.4 AC1·cAMP·PKA System ..... 15
4.3.5 CaN, PKA, PP2A·I-1·PP1 System ..... 15
Part C: Modeling of AMPAR Trafficking (Figure 1C) ..... 18
5. AMPAR Trafficking ..... 18
5.1 AMPAR Phosphorylation ..... 18
5.2 AMPAR Recycling ..... 19
Supplemental References ..... 26

## Preface

The STDP model consists of the postsynaptic membrane potential model (**Part A**), the postsynaptic signaling cascades model (**Part B**) and the AMPAR trafficking model (**Part C)**. The postsynaptic membrane potential model consists of a postsynaptic neuron model and pre- and postsynaptic stimulation models, and the postsynaptic signaling cascades model consists of $Ca^{2+}$ influx/removal model and the intracellular signaling cascades model. All simulations were executed on the GENESIS simulator with kinetikit interface (Bhalla and Iyengar, 1999), and stimulations were run after 500 s-pre-run to reach an equilibrium state. Throughout the simulations, the exponential Euler method with inhomogeneous and adaptive integration time step was used for stable and precise computation. The constructed programs are available for download at http://www.kurodalab.org/info/STDP/index.html. All details of the model are stated in the following sections.

# Part A: Modeling of Postsynaptic Membrane Potential (Figure 1A)

## 1. Postsynaptic Neuron

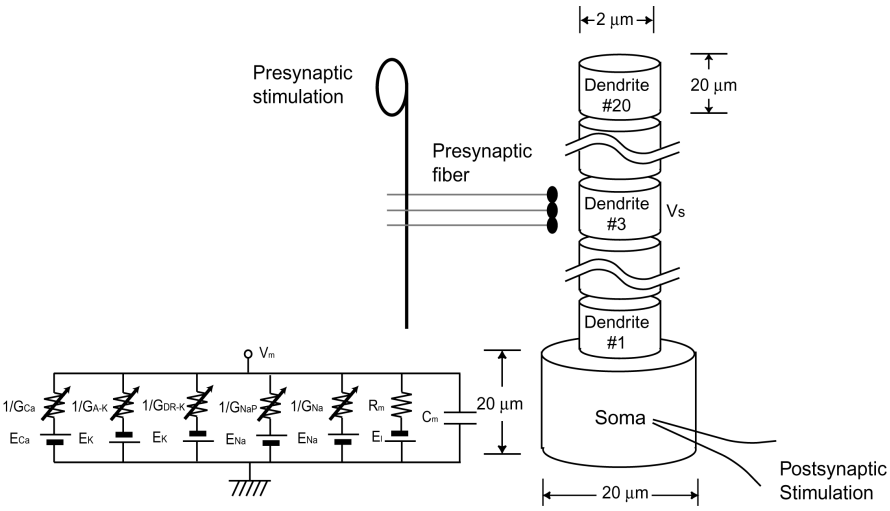


**Figure SI1**

We constructed a multi-compartment model of a postsynaptic neuron with Hodgkin-Huxley like channel kinetics, and estimated membrane potential in responses to pre- and postsynaptic stimulation on the basis of rat hippocampal CA1 neurons (**Figure SI1**) (Migliore et al., 1999; Poirazi et al., 2003). In experiments, a presynaptic stimulus depolarizes a postsynaptic site, whereas a postsynaptic spike, triggered by current injection to soma, backwardly propagates into dendrites and depolarizes the postsynaptic site. NMDARs and VGCCs at the synaptic site detect the depolarization $V_s$ and determine the postsynaptic $Ca^{2+}$ influx. To model these phenomena, one somatic and 20 dendritic compartments were sequentially connected with the indicated lengths and diameters (**Figure SI1**). Then spike-generating $Na^+$, persistent $Na^+$, delayed rectifier $K^+$, A-type $K^+$ and L-type voltage gated $Ca^{2+}$ channels were inserted with a variety of densities (see sections 1.1 – 1.4). The synaptic site was assumed to be 60 μm apart from the soma (3rd dendritic compartment from the soma). We omitted a compartment representing the postsynaptic spine in the present study, because membrane potentials of the postsynaptic spine and the parent dendrite were almost the same in our preliminary simulation.

The passive properties of the model neuron were as follows. Intracellular resistivity $R_i$ was 0.15 kΩcm, membrane resistivity $R_m$ was 28 kΩcm$^2$ for axon and soma (14 kΩcm$^2$, for dendrites), and membrane capacitance $C_m$ was $1 \times 10^3$ nF/cm$^2$ for axon and soma ($2 \times 10^3$ nF/cm$^2$ for dendrites). These parameters gave a

membrane potential decay constant of $28 \times 10^{-3}$ s. The equilibrium potential of leak channels $E_m$ was adjusted to maintain a –65-mV resting membrane potential for each compartment. All data were taken from the published literature (Migliore et al., 1999; Golding et al., 2001; Poirazi et al., 2003).

Kinetics and distributions of spike-generating $Na^+$, persistent $Na^+$, delayed rectifier $K^+$, A-type $K^+$, and L-type voltage gated $Ca^{2+}$ channels, as well as kinetics of pre- and postsynaptic stimulation, are described in the following subsections. The equilibrium potentials of $Na^+$ channels $E_{Na}$, $K^+$ channels $E_K$, AMPAR channels $E_{AMPAR}$, and NMDAR channels $E_{NMDAR}$ were 55 mV, –90 mV, 0mV and 0mV, respectively. Time, voltage, conductance and current units in the subsections are 's', 'mV', 'mS/cm$^2$' and 'μA/cm$^2$', respectively.

### 1.1 Spike-Generating $Na^+$ Current $I_{Na}$

Spike-generating $Na^+$ channel kinetics for $I_{Na}$ are given by

$$I_{Na}(t,V) = \bar{g}_{Na} m^2 h i (E_{Na} - V),$$

$$\frac{dm}{dt} = \frac{1}{5\times10^{-5}}\left[\frac{1}{1+\exp(-(V+40)/3)} - m\right],$$

$$\frac{dh}{dt} = \frac{1}{5\times10^{-4}}\left[\frac{1}{1+\exp((V+45)/3)} - h\right],$$

$$\frac{di}{dt} = \frac{1}{\tau_i}\left[\frac{1+Na_{att}\cdot\exp((V+60)/2)}{1+\exp((V+60)/2)} - i\right],$$

$$\tau_i = \max\left[\frac{\exp(0.08897(V+60))}{0.3\left[1+\exp(0.4448(V+60))\right]}, 3\times10^{-3}\right],$$

where $\bar{g}_{Na}$ is the peak conductance density, *m, h* and *i* are the gate functions of activation, inactivation and slow inactivation, respectively, and $Na_{att}$ is the dendritic inactivation factor in repetitive spiking. The gate function *i* represents attenuation of spike amplitudes in high frequency bursts, which has been experimentally shown to be small at the soma and high in distal dendrites (Migliore, 1996). Here, $\bar{g}_{Na}$ = 7 mS/cm$^2$ for soma and dendrites, and $Na_{att}$ is defined by

$$Na_{att} = \begin{cases} 0.95 & (0 \le d < 50) \\ -2.6\times10^{-3} d + 1.08 & (50 < d \le 300) \\ 0.30 & (300 < d) \end{cases},$$

where *d* (μm) is the dendritic distance from the soma. The kinetics and distributions were taken from the literature (Migliore et al., 1999; Poirazi et al., 2003).

### 1.2 Delayed-Rectifier $K^+$ Current $I_{DR\text{-}K}$

Delayed-rectifier $K^+$ channel kinetics for $I_{DR\text{-}K}$ are given by

$$I_{\text{DR-K}}(t,V) = \bar{g}_{\text{DR-K}} m^2 (E_{\text{K}} - V),$$

$$\frac{dm}{dt} = \begin{cases} \dfrac{1}{3.5\times10^{-3}}\left[\dfrac{1}{1+\exp(-(V+46.3)/3)} - m\right] & \text{for soma} \\ \dfrac{1}{2.2\times10^{-3}}\left[\dfrac{1}{1+\exp(-(V+42)/2)} - m\right] & \text{for dendrite} \end{cases},$$

where $\bar{g}_{\text{DR-K}}$ is the peak conductance density. Here, $\bar{g}_{\text{DR-K}}$ were 1.4 mS/cm$^2$ and 0.867 mS/cm$^2$ for soma and dendrites, respectively (Poirazi et al., 2003).

### 1.3 A-Type $K^+$ Current $I_{\text{A-K}}$

A-type $K^+$ channel kinetics of proximal dendrites (under 100 μm from soma) for $I_{\text{A-Kprox}}$ is given by

$$I_{\text{A-Kprox}}(t,V) = \bar{g}_{\text{A-K}} mh(E_{\text{K}} - V),$$
$$\frac{dm}{dt} = \frac{0.25(1+\alpha)}{\beta\times10^{-3}}\left[\frac{1}{1+\alpha} - m\right],$$
$$\alpha = \exp\left[0.03707k(V-11)\right],$$
$$\beta = \exp\left[0.02039k(V-11)\right],$$
$$k = -1.5 - 1\Big/\left(1+\exp\left[(V+40)/5\right]\right),$$
$$\frac{dh}{dt} = \frac{1}{\tau_h}\left[\frac{1}{1+\exp\left[0.1112(V+56)\right]} - h\right],$$
$$\tau_h = \max\left[2.6(V+50)\times10^{-4}, 2\times10^{-3}\right],$$

where $\bar{g}_{\text{A-K}}$ is the peak conductance density. Also, A-type $K^+$ channel kinetics of distal dendrites (over 100 μm from soma) for $I_{\text{A-Kdist}}$ is given by

$$I_{\text{A-Kdist}}(t,V) = \bar{g}_{\text{A-K}} mh(E_{\text{K}} - V),$$
$$\frac{dm}{dt} = \frac{0.5(1+\alpha)}{\beta\times10^{-3}}\left[\frac{1}{1+\alpha} - m\right],$$
$$\alpha = \exp\left[0.03707k(V+1)\right],$$
$$\beta = \exp\left[0.01446k(V+1)\right],$$
$$k = -1.8 - 1\Big/\left(1+\exp\left[(V+40)/5\right]\right),$$
$$\frac{dh}{dt} = \frac{1}{\tau_h}\left[\frac{1}{1+\exp\left[0.1133(V+56)\right]} - h\right],$$
$$\tau_h = \max\left[2.6(V+50)\times10^{-4}, 2\times10^{-3}\right].$$

Here, $\bar{g}_{\text{A-K}}$ is given by

$$\bar{g}_{A\text{-}K} = \begin{cases} 7.5 & (0 \le d < 100) \\ 48.67 \cdot d/350 & (100 < d \le 350) \\ 48.67 & (350 < d) \end{cases},$$

where $d$ (μm) is the dendritic distance from the soma. A-type $K^+$ channels suppress backpropagating APs in distal dendrites, and conversely amplify the APs via inactivation of the $h$ gate when APs and EPSPs are coincided at pre- $\rightarrow$ post-spiking (Hoffman et al., 1997). The kinetics and distributions were taken from the literature (Migliore et al., 1999; Poirazi et al., 2003).

### 1.4 L-type Voltage-Gated $Ca^{2+}$ Channel $I_{L\text{-}Ca}$

L-type $Ca^{2+}$ channel kinetics $I_{L\text{-}Ca}$ is given by

$$I_{\text{L-Ca}}(t,V) = \bar{g}_{\text{L-Ca}} m^3 h \frac{V}{1-\exp(\phi V)},$$

$$\frac{dm}{dt} = \frac{1}{3.6\times10^{-3}}\left[\frac{1}{1+\exp(-(V+37))} - m\right],$$

$$\frac{dh}{dt} = \frac{1}{2.9\times10^{-2}}\left[\frac{1}{1+\exp((V+41)/0.5)} - h\right],$$

where $\phi$ = 0.0756 $mV^{-1}$, and $\bar{g}_{\text{L-Ca}}$ is the peak conductance density. $\bar{g}_{\text{L-Ca}}$ is given by

$$\bar{g}_{\text{L-Ca}} = \begin{cases} 93 & (\text{soma}) \\ 146 & (0 < d \le 50) \\ 3.2 & (50 < d) \end{cases},$$

where $d$ (μm) is the dendritic distance from the soma. L-type $Ca^{2+}$ channels enlarge the half-width of backpropagating APs as observed in experiments (Golding et al., 2001), and contribute to the possible occurrence of $Ca^{2+}$-channel mediated dendritic spikes (Golding et al., 1999). Prolonged APs are important for sufficient $Ca^{2+}$ influx via NMDARs with $Mg^{2+}$-unblock at pre- $\rightarrow$ post-spiking (Neville and Lytton, 1999). The derivation of voltage dependence for $Ca^{2+}$ current is described in the section about "$Ca^{2+}$ influx and removal."

## 2. Pre- and Postsynaptic Stimulation

### 2.1 Neurotransmitter Release by Presynaptic Stimulation

Presynaptic stimulation stimulates postsynaptic receptors via probabilistic release of neurotransmitter (glutamate) from presynaptic terminal. The probability of glutamate release depends on preceding glutamate releases, and STDP depends on the probabilistic release (Tsodyks and Markram, 1997; Froemke et al., 2006). Here, we formulated the probabilistic glutamate release at a synapse, $P(t)$, to estimate $Ca^{2+}$

influx via NMDARs, as follows (Matveev and Wang, 2000) :

$$\begin{aligned} P(t) &= 1-\exp\left[-\alpha N(t)\right], \\ N(t) &= \max\left[0, N_0 - \sum_{t>t_j^{syn}} v(t-t_j^{syn})\right], \\ v(t') &= \exp(-t'/\tau_D)\cdot H(t'), \end{aligned}$$

where $N_o$ is the maximum vesicle number, $\alpha$ is the fusion rate constant, $\tau_D$ is the recovery time constant, $t_j^{syn}$ is the time of $j^{\text{th}}$ glutamate release event, and $H(t)$ is the Heaviside step function. Here, $N_o$ = 1.1, $\alpha$ = 4, and $\tau_D$ = 0.25 s. $P(t)$ is approximated to be 1 If no-presynaptic stimulation occurs over 0.5 s. When a presynaptic neuron fires at $t_i^{pre}$, glutamate release event occurs with the probability $P(t_i^{pre})$, and the event is count as $j^{\text{th}}$ glutamate release ($t_j^{syn} \leftarrow t_i^{pre}$ ).

The probabilistic release was prepared in two ways. One is the absolute release profile at a single synapse to estimate $Ca^{2+}$ influx via NMDARs. The other is the trial average (or ensemble mean) of release profiles to estimate AMPAR- and NMDAR-EPSPs, since multiple synaptic inputs are given to a postsynaptic neuron by a single stimulation of as axon bundle. The trial average is represented by $P_{rel}(t_i^{pre})$.

## 2.2 Response of Postsynaptic Receptors and the Allosteric Kinetics of NMDARs

Synaptic current is composed of AMPAR-mediated current $I_{\text{AMPAR}}$ and NMDAR-mediated current $I_{\text{NMDAR}}$. First, $I_{\text{AMPAR}}$ was modeled by using $\alpha$-function as follows:

$$I_{\text{AMPAR}}(t,V_s) = \bar{g}_{\text{AMPAR}} \sum_j P_{rel}(t_j^{\text{Pre}}) g_{\text{AMPAR}}(t-t_j^{\text{Pre}})(E_{\text{AMPAR}} - V_s)$$

$$g_{\text{AMPAR}}(t') = \frac{t'}{3\times10^{-3}} \exp\left[1-\frac{t'}{3\times10^{-3}}\right]\cdot H(t'),$$

where $\bar{g}_{\text{AMPAR}}$ is the peak conductance, $P_{rel}(t_i^{pre})$ is the trial average of release profiles, $t_j^{\text{Pre}}$ is time at $j^{\text{th}}$ presynaptic stimulus (s), $E_{\text{AMPAR}}$ is the equilibrium potential, and $H(t)$ is the Heaviside step function. Here $\bar{g}_{\text{AMPAR}}$ = 0.3 nS, and $E_{\text{AMPAR}}$ = 0 mV. $I_{\text{AMPAR}}$ is the ensemble of multiple synaptic inputs from stimulated axon bundles.

Next, $I_{\text{NMDAR}}$ was modeled in consideration of extracellular $Mg^{2+}$-block (Castellani et al., 2001) and channel open kinetics of CaM-bound and CaM-unbound NMDARs (Ehlers et al., 1996; Rycroft and Gibb, 2002) as follows:

$$I_{\text{NMDAR}}(t,V_s) = \bar{g}_{\text{NMDAR}} \cdot \left(O + O\cdot CaM\right) \cdot \frac{E_{\text{NMDAR}} - V_s}{1+([\text{Mg}^{2+}]/3.57)\exp(-0.062V_s)}$$

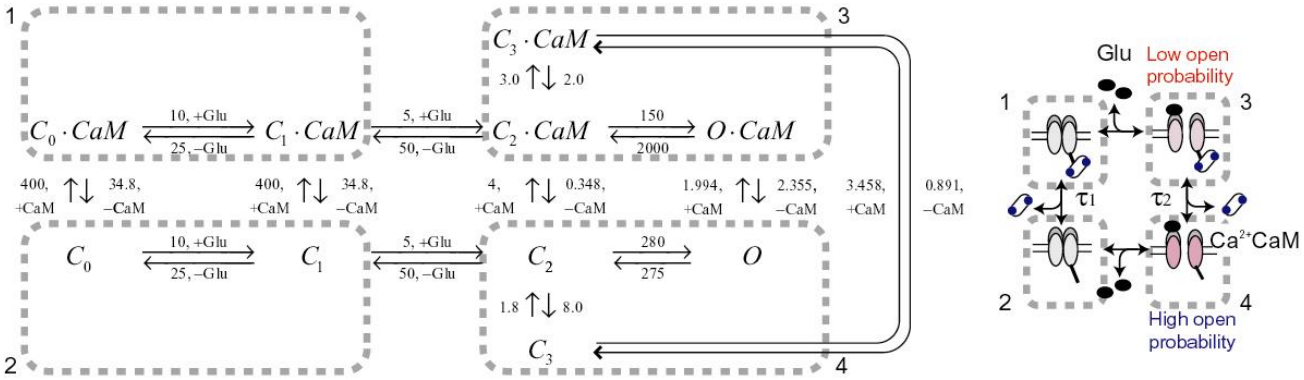


where $\bar{g}_{NMDAR}$ is the peak conductance, $E_{NMDAR}$ is the equilibrium potential, $[Mg^{2+}]$ is the concentration of extracellular $Mg^{2+}$, $C_0$, $C_1$, $C_2$, $C_3$, $C_0 \cdot CaM$, $C_1 \cdot CaM$, $C_2 \cdot CaM$, $C_3 \cdot CaM$ are the concentration of closed-state NMDAR channels, and $O$ and $O \cdot CaM$ are the concentration of open-state channels. *CaM* represents $2Ca^{2+}$·CaM or $3Ca^{2+}$CaM, and the numeric on arrows are rate constants in $\mu M^{-1}s^{-1}$ or $s^{-1}$, which were set on the basis of the experimental kinetics of NMDARs (Ehlers et al., 1996; Rycroft and Gibb, 2002) except that the affinity of Glu to NMDARs for C0 regions (87 nM) was used because the affinity to the C1 region of NMDARs was too high (4 nM) and the binding of $Ca^{2+}$·CaM to NMDARs was saturated even at the basal $Ca^{2+}$ level. Here $\bar{g}_{NMDAR}$ = 50 $nS\mu M^{-1}$, $E_{NMDAR}$ = 0 mV, $[Mg^{2+}]$ = 1.5 mM (Froemke and Dan, 2002), and the total NMDAR concentration was 1 μM. The right panel in the description of NMDAR kinetics shows the schematic representation of the allosteric kinetics of NMDARs (**Figure 4A**), where the indicated numbered bashed boxes denote corresponding components in the left panel. NMDAR binds to both $2Ca^{2+}$·CaM and $3Ca^{2+}$·CaM (James et al., 1995; Akyol et al., 2004), and the kinetics constants for "NMDAR·$2Ca^{2+}$·CaM + $Ca^{2+}$ ↔ NMDAR·$3Ca^{2+}$·CaM" is the same as those for "$2Ca^{2+}$·CaM + $Ca^{2+}$ ↔ $3Ca^{2+}$·CaM." Decrease of free $nCa^{2+}$·CaM concentration by binding to NMDARs was omitted for simplicity. Here, the time constants of the transition of $Ca^{2+}$·CaM -unbound and –bound NMDARs were set at 230 and 2.3 ms, respectively, under the condition where CaM was 1 μM. All the kinetic constants were set to satisfy the principle of detailed balance in thermodynamics equilibrium.

States of NMDAR channels are discontinuously changed at the time of presynaptic stimulation ($t_i^{pre}$), because the glutamate release by presynatic stimulation is a flash event (~ 100 μs) (Clements, 1996). The update equation is given by:

$$C_0 \leftarrow C_0 \cdot e^{-10\cdot \mathrm{Glu}_{tot}}$$
$$C_1 \leftarrow 2C_0 \left\{ e^{-5\cdot \mathrm{Glu}_{tot}} - e^{-10\cdot \mathrm{Glu}_{tot}} \right\} + C_1 \cdot e^{-5\cdot \mathrm{Glu}_{tot}}$$
$$C_2 \leftarrow C_0 \left\{ 1 + e^{-10\cdot \mathrm{Glu}_{tot}} - 2e^{-5\cdot \mathrm{Glu}_{tot}} \right\} + C_1 \left\{ 1 - e^{-5\cdot \mathrm{Glu}_{tot}} \right\} + C_2$$
$$C_0 \cdot CaM \leftarrow C_0 \cdot CaM \cdot e^{-10\cdot \mathrm{Glu}_{tot}}$$
$$C_1 \cdot CaM \leftarrow 2C_0 \cdot CaM \left\{ e^{-5\cdot \mathrm{Glu}_{tot}} - e^{-10\cdot \mathrm{Glu}_{tot}} \right\} + C_1 \cdot CaM \cdot e^{-5\cdot \mathrm{Glu}_{tot}}$$
$$C_2 \cdot CaM \leftarrow C_0 \cdot CaM \left\{ 1 + e^{-10\cdot \mathrm{Glu}_{tot}} - 2e^{-5\cdot \mathrm{Glu}_{tot}} \right\} + C_1 \cdot CaM \left\{ 1 - e^{-5\cdot \mathrm{Glu}_{tot}} \right\} + C_2 \cdot CaM$$

where $\mathrm{Glu}_{tot}$ is the total intensity of released glutamate. Here $\mathrm{Glu}_{tot} = 0.4 \times P_{rel}(t_i^{pre})$ μM·s. The discontinuous update is calculated from the second order glu-binding reactions and the temporal pattern of glutamate release $Glu(t)$:

$$C_0 \xrightarrow{10Glu(t)} C_1 \xrightarrow{5Glu(t)} C_2 ,$$
$$C_0 \cdot CaM \xrightarrow{10Glu(t)} C_1 \cdot CaM \xrightarrow{5Glu(t)} C_2 \cdot CaM ,$$
$$\frac{dC_0}{dt} = -10Glu(t)C_0, \quad \frac{dC_1}{dt} = 10Glu(t)C_0 - 5Glu(t)C_1, \quad \frac{dC_2}{dt} = 5Glu(t)C_1,$$
$$\frac{dC_0 \cdot CaM}{dt} = -10Glu(t)C_0 \cdot CaM,$$
$$\frac{dC_1 \cdot CaM}{dt} = 10Glu(t)C_0 \cdot CaM - 5Glu(t)C_1 \cdot CaM,$$
$$\frac{dC_2 \cdot CaM}{dt} = 5Glu(t)C_1 \cdot CaM,$$

where $Glu(t) = \mathrm{Glu}_{tot} \lim_{\Delta t \to 0} f(\Delta t)$,

$$f(\Delta t) = \begin{cases} 0 & (t < 0) \\ 1/\Delta t & (0 \le t < \Delta t) \\ 0 & (\Delta t \le t) \end{cases} .$$

## 2.3 Postsynaptic Stimulation

Postsynaptic stimulation, a brief current injection to soma $I_{\mathrm{current}}$, was modeled using α-function as follows:

$$I_{\mathrm{current}}(t) = \bar{I}_{\mathrm{peak}} \sum_j \frac{t - t_j^{\mathrm{Post}}}{5\times 10^{-4}} \exp\left[ 1 - \frac{t - t_j^{\mathrm{Post}}}{5\times 10^{-4}} \right] \cdot H(t - t_j^{\mathrm{Post}}) ,$$

where $\bar{I}_{\mathrm{peak}}$ is the peak current, and $t_j^{\mathrm{Post}}$ is time at $j^{\mathrm{th}}$ postsynaptic stimulus (s). Here $\bar{I}_{\mathrm{peak}}$ = 0.5 nA, which was sufficient to induce an action potential.

## Part B: Modeling of Postsynaptic Signaling Cascades (Figure 1B)

## 3. $Ca^{2+}$ Influx and Removal

We modeled $Ca^{2+}$ influx to a spine via NMDARs and VGCCs as well as $Ca^{2+}$ removal from the spine, and estimated postsynaptic $Ca^{2+}$ concentration $[Ca^{2+}]_i$ in responses to pre- and postsynaptic stimulation (**Figure SI2**). Presynaptic stimulation activates AMPARs and NMDARs, and leads to $Ca^{2+}$ influx mainly via NMDARs including the effect of $Mg^{2+}$ unblock by EPSPs. Postsynaptic stimulation induces an AP, and the depolarization signal leads to $Ca^{2+}$ influx via VGCCs. Increased $[Ca^{2+}]_i$ is removed by $Ca^{2+}$ pump, and returns to the basal level (Sabatini et al., 2001).

We set NMDARs, VGCCs, and $Ca^{2+}$ pump distributed in the membrane of a postsynaptic spine (Sabatini et al., 2002). Generally, $Ca^{2+}$ influx $j^{Ca}_X$ (nmol·s$^{-1}$·cm$^{-2}$) through channel $X$ is obtained from the Goldman-Hodgkin-Katz current equation $i^{Ca}_X$, which is dependent on postsynaptic membrane potential $V_s$, $[Ca^{2+}]_i$ and extracellular $Ca^{2+}$ concentration $[Ca^{2+}]_o$, as follows:

$$\begin{aligned} j_X^{\mathrm{Ca}} &= \frac{i_X^{\mathrm{Ca}}}{2F} \\ &= -\frac{p_X^{\mathrm{Ca}} \phi V_S \left\{ [\mathrm{Ca}^{2+}]_o - [\mathrm{Ca}^{2+}]_i \exp(\phi V_S) \right\}}{1-\exp(\phi V_S)} \\ &\sim -\frac{P_X^{\mathrm{Ca}} V_S}{1-\exp(\phi V_S)} \end{aligned}$$

where $p^{Ca}_X$ is the permeability of channel $X$, $P^{Ca}_X = 2\phi\, p^{Ca}_X [Ca^{2+}]_o$ (nmol·s$^{-1}$·mV$^{-1}$·cm$^{-2}$), and $\phi$ is $2F/RT$, where $F$ is Faraday's constant, $R$ is the gas constant, and $T$ is the absolute temperature. Here $\phi$ = 0.0756 mV$^{-1}$, and the component $[Ca^{2+}]_i/[Ca^{2+}]_o \exp(-2\phi V_s)$ was omitted in consideration of $[Ca^{2+}]_o >> [Ca^{2+}]_i$. Because we focused on NMDAR-dependent LTP and LTD, we omitted metabotropic glutamate receptor-dependent intracellular $Ca^{2+}$ release to avoid unnecessary complexity.

### 3.1 $Ca^{2+}$ Influx via NMDARs

$Ca^{2+}$ permeability of NMDARs with voltage-dependent $Mg^{2+}$ block (Castellani et al., 2001), $P^{Ca}_{NMDAR}$, is given by

$$P^{\mathrm{Ca}}_{\mathrm{NMDAR}}(V,t) = \bar{P}_{\mathrm{NMDAR}} \left( O + O \cdot CaM \right) \frac{1}{1 + ([\mathrm{Mg}^{2+}]/3.57)\exp(-0.062 V_S)}$$

where $[Mg^{2+}]$ is the concentration of extracellular $Mg^{2+}$, $\bar{P}_{NMDAR}$ is the maximum channel permeability of NMDARs, and $O$ and $O{\cdot}CaM$ are the concentrations of open-state NMDAR channels where the discontinuous update by glutamate release occurs at $t_j^{syn}$ with $Glu_{tot}$ = 0.4 μM·s (see above). Here, $[Mg^{2+}]$ = 1.5 mM (Froemke and Dan, 2002). We set $\bar{P}_{NMDAR}$ = 0.5, 1, 2.5, and 2.5 nmol·s$^{-1}$·mV$^{-1}$·cm$^{-2}$ in the

allosteric model, the no-allosteric model with slow suppression, the no-allosteric model with rapid suppression, and the allosteric model with opposite time constants ($\tau_1$ = 230 ms, $\tau_2$ = 2.3 ms), respectively, not to induce potentiation nor depression by uncorrelated pre- and post-spiking. NMDARs were distributed in the membrane of the PSD compartment (shown below), and the maximum permeability produces 1 μM-peak $Ca^{2+}$ at the cytosolic compartment by a single presynaptic stimulation (Sabatini et al., 2002).

### 3.2 $Ca^{2+}$ Influx via VGCCs

The permeability of high voltage activated L-type VGCCs, $P^{Ca}_{VGCC}$, is given by

$$P^{\mathrm{Ca}}_{\mathrm{VGCC}}(V,t) = \bar{P}_{\mathrm{VGCC}} m^3 h \frac{V}{1-\exp(\phi V)},$$

$$\frac{dm}{dt} = \frac{1}{0.0036}\left[\frac{1}{1+\exp(-(V+37))} - m\right],$$

$$\frac{dh}{dt} = \frac{1}{0.029}\left[\frac{1}{1+\exp((V+41)/0.5)} - m\right],$$

where $\bar{P}_{\mathrm{VGCC}}$ is the maximum channel permeability of VGCCs ( $\bar{P}_{\mathrm{VGCC}}$ = 0.04 nmol·s$^{-1}$·mV$^{-1}$·cm$^{-2}$). L-type $Ca^{2+}$ channels in spines play specific roles in inducing STDP (Bi and Poo, 1998; Peng et al., 2004; Froemke et al., 2005).

### 3.3 $Ca^{2+}$ Removal

Removal of free $Ca^{2+}$ by $Ca^{2+}$ pump in the membrane $j^{Ca}_{pump}$ (nmol·s$^{-1}$·cm$^{-2}$) is simply given by

$$j^{Ca}_{pump} = 0.8\left([\mathrm{Ca}^{2+}]_{rest} - [\mathrm{Ca}^{2+}]_i\right)$$

where $[Ca^{2+}]_{rest}$ is the basal $Ca^{2+}$ concentration. Here, $[Ca^{2+}]_{rest}$ = 0.05 μM. The $Ca^{2+}$ pump decreases elevating $[Ca^{2+}]_i$ in a double exponential manner, consisting of a 3-ms fast component for free $Ca^{2+}$ and a 30-ms slow component for CaM-interacting $Ca^{2+}$ (Sabatini et al., 2002).

## 4. Intracellular Signaling Cascades

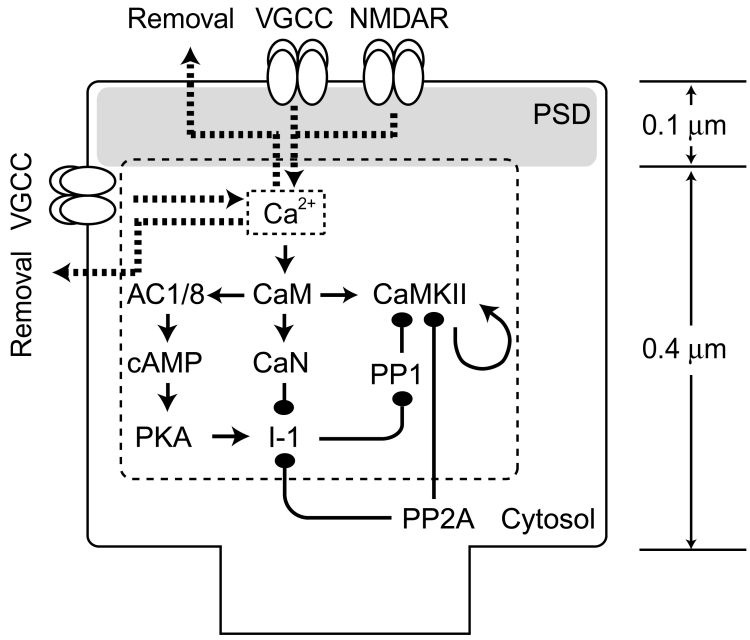


**Figure SI2**

We set the framework of biochemical intracellular signaling cascades within a spine on the basis of the earlier models (Bhalla and Iyengar, 1999; Kuroda et al., 2001; Doi et al., 2005) and observations (**Figure SI2**) (Winder and Sweatt, 2001; Lisman et al., 2002). We tried to make an essential and rather simple model of intracellular signaling cascades to avoid redundancy and unnecessary complexity. The intracellular signaling cascades involves the $Ca^{2+}$-dependent activation of CaMKII (see sections 4.3.1, 4.3.2), PKA via AC1/8 (4.3.4) and CaN (4.3.3). CaMKII activation also involves its autophosphorylation by itself or neighboring subunits. PP1 and PP2A dephosphorylates CaMKII. PKA phosphorylates I-1, and CaN and PP2A dephosphorylates it (4.3.5). Phosphorylated I-1 binds PP1 and inactivates it (4.3.5). Therefore, PP1 activation and inactivation depend on CaN and PP2A, and on PKA, respectively. CaMKII, and PP1 and PP2A phosphorylates and dephosphorylates AMPARs, respectively, whose trafficking depends (see below; 5. Modeling of AMPAR trafficking).

We set a spine as a cylinder, which is 0.5 μm long and has a 0.2-$\mu m^2$ section area (Stuart et al., 1999). The spine was divided into the PSD and cytosol compartments with 0.1-μm and 0.4-μm lengths, respectively (**Table SIa**). We assumed that all molecules as indicated by the dashed box (except PP2A that exists only in the cytosol) diffuse between PSD and cytosol (see below), because PP2A is reportedly not enriched in the PSD fraction (Strack et al., 1997). The localization of these

molecules at PSD fraction implicitly represents their bindings to scaffold proteins such as PSD95, SAP97 and AKAP (Halpain et al., 1998; Wang et al., 2002; Petersen et al., 2003; Bauman et al., 2004; Bordelon et al., 2005). We assumed that the molecules within each compartment were well mixed, and that they deterministically interacted on the basis of mass assumption. The detailed interactions are described below.

### 4.1 Formalization of Molecular Interaction

All interactions in the signal transduction pathways were represented by binding and enzymatic reactions (Bhalla and Iyengar, 1999; Doi et al., 2005). For example, a binding reaction in which A binds to B to form AB is expressed by the following equation:

$$A + B \underset{k_b}{\overset{k_f}{\rightleftarrows}} AB ,$$

where $k_f$ and $k_b$ are the rate constants for the forward and backward reactions. The rates $k_f$ and $k_b$ are generally determined by two experimentally observable constants, the dissociation constant $K_d$ and the time constant $\tau$. $K_d$ is defined as $K_d = k_b / k_f$. In turn, enzymatic reactions were modeled by the Michaelis-Menten formulation:

$$S + E \underset{k_{-1}}{\overset{k_1}{\rightleftarrows}} SE \xrightarrow{k_{cat}} P + E$$

where S, E and P denote substrates, enzymes and products, respectively. The kinetic parameters $k_1$, $k_{-1}$, and $k_{cat}$ are determined by two observable constants: the Michaelis constant $K_m$ and the maximum enzyme velocity $V_{max}$. $K_m$ is defined as $K_m = (k_{-1} + k_{cat}) / k_1$, and $V_{max}$ is defined as $V_{max} = k_{cat}[E]_{total}$, where $[E]_{total}$ is the total concentration of the enzyme. We assumed $k_{-1} / k_{cat} = 4$ for all enzymatic reactions (Bhalla and Iyengar, 1999).

### 4.2 Formalization of Molecular Diffusion

Diffusion of the signal transduction molecules was represented by the following reaction-diffusion equations:

$$\begin{aligned}\frac{\partial [X]_{cytosol}}{\partial t} &= D_X \frac{\partial^2}{\partial x^2}[X]_{cytosol} + \sum_i R^i_{X,cytosol} + \frac{S_{cytosol}}{V_{cytosol}} \sum_i j^i_{X,cytosol} \\ &\sim \frac{D_X}{(\Delta x)^2}\left\{[X]_{PSD} - [X]_{cytosol}\right\} + \sum_i R^i_{X,cytosol} + \frac{S_{cytosol}}{V_{cytosol}} \sum_i j^i_{X,cytosol}\end{aligned}$$

where $[X]_{cytosol}$ and $[X]_{PSD}$ are the concentration of molecule $X$ in cytosolic and PSD compartments, respectively, $D_X$ is the diffusion coefficient, $R_{X,cytosol}$ is the reaction components, $J_{X,cytosol}$ is the influx or removal components, and $\Delta x$ is the effective distance between cytosolic and PSD compartments. Here, we set $\Delta x = 0.15$ μm.

Diffusion coefficients $D_x$ of $Ca^{2+}$, cAMP, CaM, CaMKII, PKA, CaN and PDE were obtained from the literature, and those of I-1 and PP1 were estimated from the relationship between $D_x$ and molecular weight $M_x$ (**Table SIb**). The diffusion coefficients of complexes were assumed to take the smallest value in those of constituents for simplicity. The diffusion between a spine and a parent dendrite was not modeled, because the diffusion of fast molecular dynamics such as $Ca^{2+}$ is negligible (Sabatini et al., 2002).

### 4.3 Overview of Molecular Interactions

Notations of **Figures SI3** and **SI4**: Circles and boxes with arrows denote molecule-molecule interactions and enzymatic reactions, respectively. Rate constants (Numbered circles or boxes) and concentrations of molecules are shown in **Tables SIa–SIj**.

#### 4.3.1 $Ca^{2+}$·CaM Interaction

$Ca^{2+}$ binding kinetics of CaM has extensively been analyzed (Linse et al., 1991; Holmes, 2000). CaM binds to four $Ca^{2+}$ ions, but two or three $Ca^{2+}$-binding is enough to activate CaM (James et al., 1995; Chin and Means, 2000). For simplicity, $3Ca^{2+}$·CaM is assumed to be an active form, and reactions for $4Ca^{2+}$·CaM are omitted. The description of kinetic constants is shown in **Figure SI3** and **Tables SIc and SId**.

#### 4.3.2 $Ca^{2+}$·CaM·CaMKII System

$Ca^{2+}$·CaM binds to each subunit of a holoenzyme of CaMKII, and $Ca^{2+}$·CaM-bound subunits are phosphorylated at Thr286 by active neighboring subunits, which are $Ca^{2+}$·CaM-bound and/or Thr286 phosphorylated subunits. $Ca^{2+}$·CaM induced successive autophosphorylation of CaMKII subunits (De Koninck and Schulman, 1998), leading to the persistent activation of CaMKII (Fukunaga et al., 1993; Shen et al., 2000). On the basis of the previous CaMKII model (Dupont et al., 2003), we expanded the model for treatment of $Ca^{2+}$·CaM-, $2Ca^{2+}$·CaM-, and $3Ca^{2+}$·CaM-bound states (**Figure SI3**), and further modified the binding constants between bare CaM and the inactive subunit in consideration of experimentally observed basal activity (Fukunaga et al., 1993; Kawaguchi and Hirano, 2002). This modification also implicitly represents CaMKII by binding to NMDARs (Bayer et al., 2001; Leonard et al., 2002). The modified CaMKII shows bistable activity as a balance with PP1 activity. The present CaMKII model calculated the phosphorylation rate by active neighbors from the fraction of active subunits approximately (Dupont et al., 2003). The diffusion of active form of CaMKII from the PSD fraction is set lower than that of inactive form, because the active form of CaMKII accumulates at the PSD fraction (Strack et al., 1997; Shen et al., 2000).

The CaMKII activation inhibited by PP1 and PP2A activities, which dephosphorylate the Thr286 site of CaMKII (**Figure SI3**; **Table SIe**). PP2A exist only in the cytosol compartment (Strack et al., 1997). The description of kinetic constants is shown in **Figure SI3** and **Tables SIc–SIe**.

#### 4.3.3 CaN System

A regulatory subunit of CaN binds $4Ca^{2+}$, and a catalytic subunit of CaN binds $Ca^{2+}$·CaM. CaN activation depends on both $Ca^{2+}$ and $Ca^{2+}$·CaM (Hubbard and Klee, 1987; Kakalis et al., 1995; Klee et al., 1998; Groth et al., 2003). Because one of the $Ca^{2+}$ sites is always saturated and the other has no functional role in CaN activation, we assumed that both the rest of the $2Ca^{2+}$-binding and $Ca^{2+}$CaM-binding are responsible for the CaN activation (Feng and Stemmer, 2001; Gallagher et al., 2001). The description of kinetic constants is shown in **Figure SI4** and **Tables SIc and SIh**.

#### 4.3.4 AC1·cAMP·PKA System

AC1/8 is activated by $3Ca^{2+}$·CaM, and catalyses ATP into cAMP, which is converted into 5'-AMP by an active form of PDE (Xia and Storm, 1997; Cooper, 2003). PKA consists of two regulatory subunits, R (RII), and two catalytic subunits, C. A regulatory subunit of PKA has two cAMP-binding sites, A and B. Binding of cAMP at the site A requires the prior binding of cAMP to the site B. Conjunctive binding of 4 cAMP to 2R leads to successive dissociation of C, which is an active form (Taylor et al., 1990; Nguyen and Woo, 2003). The description of kinetic constants is shown in **Figure SI4** and **Tables SIc,SIf and SIg**.

#### 4.3.5 CaN, PKA, PP2A·I-1·PP1 System

I-1 is phosphorylated by active form of PKA, and phosphorylated I-1 is dephosphorylated by active forms of PP2A and CaN (Price and Mumby, 1999). Phosphorylated I-1 binds to PP1 and inactivates it (Huang et al., 1999; Huang and Paudel, 2000). The description of kinetic constants is shown in **Figure SI4** and **Tables SIi and SIj**.

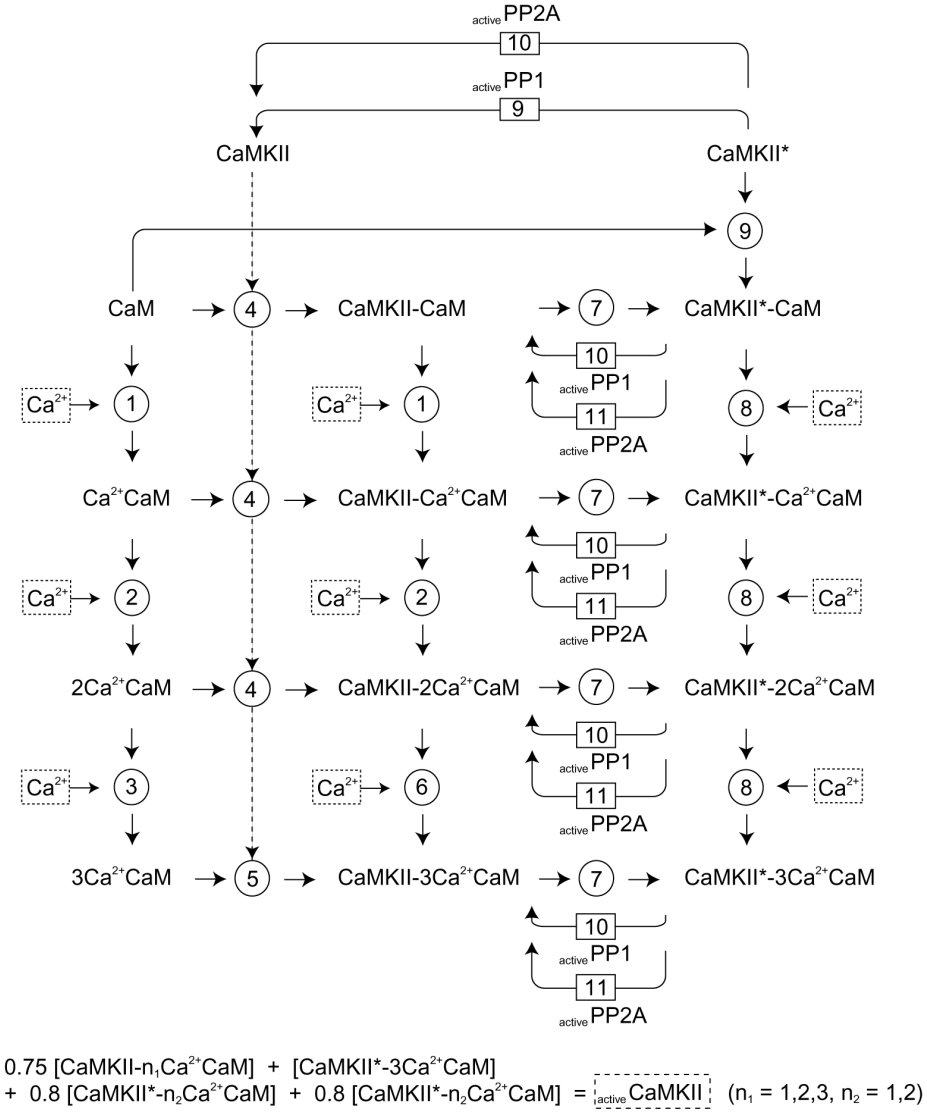


**Figure SI3.** $Ca^{2+}$·CaM·CaMKII system

Circles and boxes with arrows denote molecule-molecule interactions and enzymatic reactions, respectively. Concentrations of molecules are shown in **Table SIc**, and rate constants (Numbered circles or boxes) are shown in **Tables SId and SIe**.

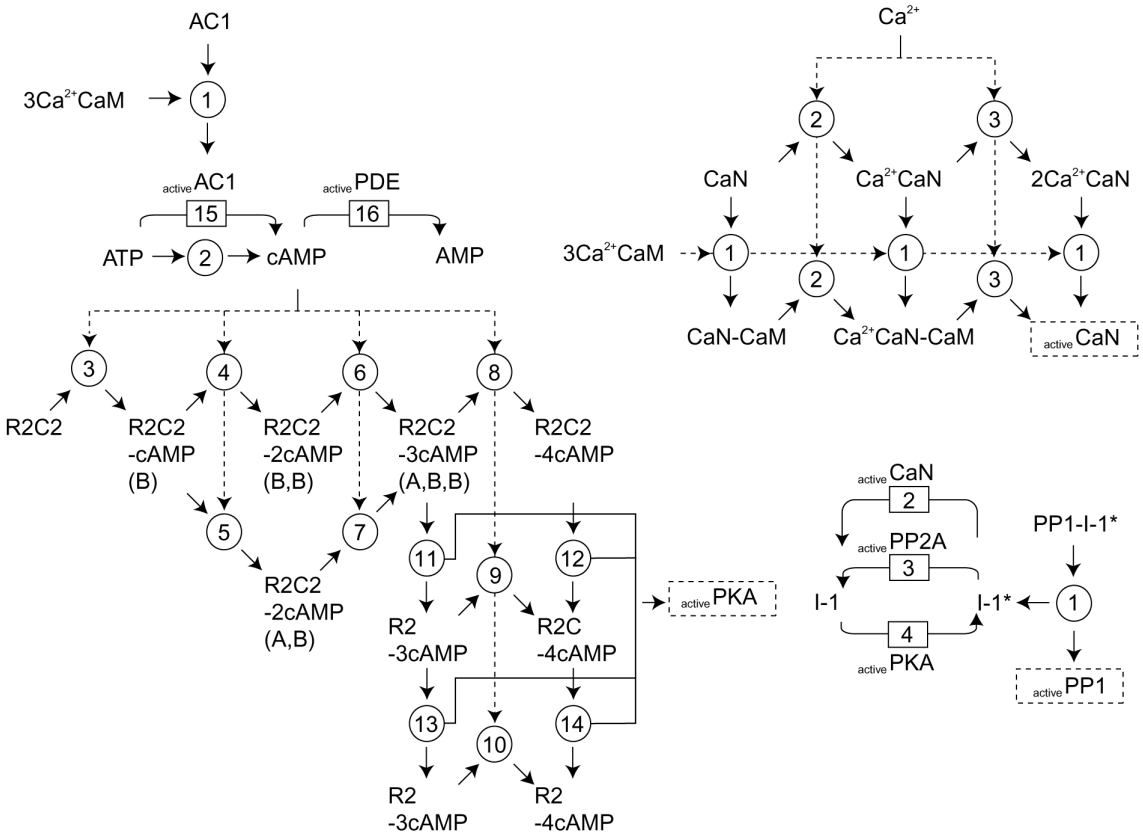


**Figure SI4.** AC1·cAMP·PKA system (left), CaN system (top right) and I-1 system (bottom right)

Circles and boxes with arrows denote molecule-molecule interactions and enzymatic reactions, respectively. Concentrations of molecules are shown in **Table SIc**, and rate constants (Numbered circles or boxes) are shown in **Tables SIf–SIj**.

# Part C: Modeling of AMPAR Trafficking (Figure 1C)

## 5. AMPAR Trafficking

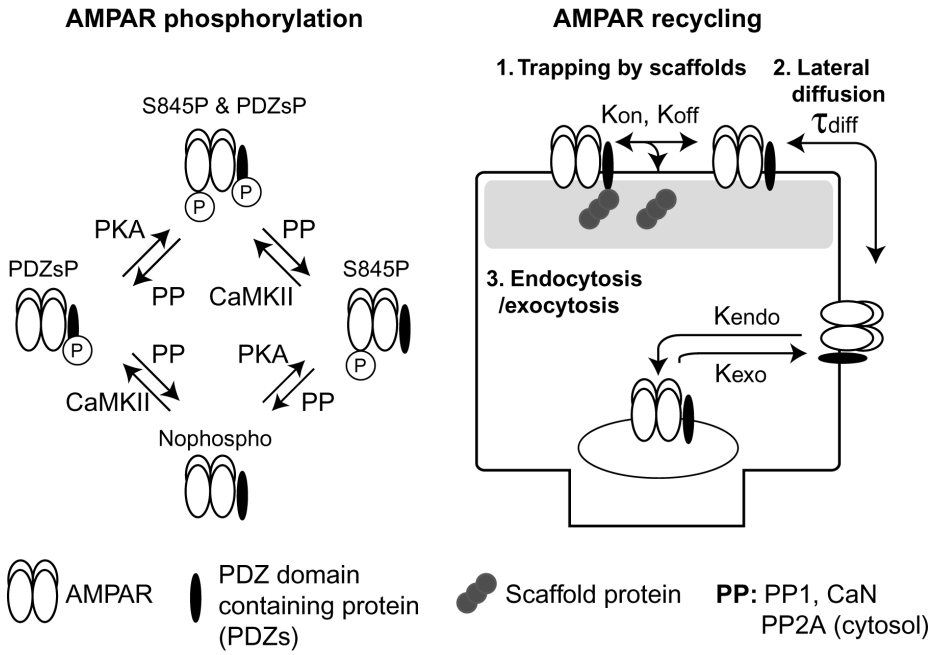


**Figure SI5**

On the basis of the recent progress in AMPARs trafficking (Malinow and Malenka, 2002; Collingridge et al., 2004), we constructed a simplified model of phosphorylation-dependent AMPAR trafficking because the detailed mechanism remains unknown (**Figure SI5**). The AMPAR trafficking model consists of AMPAR phosphorylation and recycling models. We represented GluR1, rather than GluR2/3, as AMPARs in the STDP model because LTP and LTD can be elicited in GluR2 (-/-) and GluR3 (-/-) mice (Meng et al., 2003).

### 5.1 AMPAR Phosphorylation

AMPAR is complexed with PDZ-containing scaffold proteins (PDZs), such as SAP97 and stargazin (Sans et al., 2001; Vandenberghe et al., 2005). PDZs are phosphorylated by CaMKII (Mauceri et al., 2004; Tomita et al., 2005). AMPARs are phosphorylated by PKA at Ser845. Phosphorylated AMPARs and PDZs are dephosphorylated by PP1 and CaN (Lee et al., 2000; Snyder et al., 2003). Because rate constants regarding these phosphorylation and dephosphorylation have yet to be determined, we here redefined the enzymatic reactions with the simple formulation as follows:

$$S \xrightarrow{E} P$$

$$\frac{d[S]}{dt} = -K_{\mathrm{f}}[E][S]$$
$$\frac{d[P]}{dt} = K_{\mathrm{f}}[E][S]$$

where $K_f$ is the reaction rate constant, and S, E and P denote substrates, enzymes, and products, respectively. This formulation implicitly assumes the relatively low concentration of enzyme·substrate complex, or high $K_m$ in the standard formulation of enzymatic reactions (Sasagawa et al., 2005). The unique constants, $K_f$, were determined to reproduce the ratio of the phosphorylated and unphosphorylated AMPARs in the naïve state and the phosphorylation/dephosphorylation rate of AMPARs in experimental observation. The description of kinetic constants are shown in **Figure SI5** and **Table SIk**.

### 5.2 AMPAR Recycling

AMPAR recycling contains three processes; trapping by scaffold, lateral diffusion and endocytosis/exocytosis (Malinow and Malenka, 2002; Collingridge et al., 2004). The phosphorylated PDZs associated with AMPARs and the non-phosphorylated one strongly and weakly interact with scaffold proteins at PSD, respectively, which were here assumed as cytoskeletal anchors such as PSD-95 attached with F-actin and Myosin VI (Kim and Sheng, 2004). Therefore, phosphorylation of PDZs results in stabilization of AMPARs at PSD, and the dephosphorylation results in the dissociation from PSD (Shi et al., 1999; Hayashi et al., 2000; Triller and Choquet, 2005). Any form of AMPARs laterally diffuses between the PSD membrane and the plasma membrane (Triller and Choquet, 2005). The dephosphorylated AMPARs (GluR1s at Ser845) are rapidly internalized into endosome, whereas the phosphorylated AMPARs are slowly internalized (Carroll et al., 2001; Cousin and Robinson, 2001; Blanpied et al., 2002; Kittler et al., 2005; Tigaret et al., 2006). In addition, the phosphorylated AMPARs, but not dephosphorylated form, are reinserted into the plasma membrane (Ehlers, 2000; Esteban et al., 2003).

Here, the phosphorylation-dependent increase of AMPAR numbers trapping by scaffold at PSD corresponds to the increase of synaptic conductance (LTP), whereas the dephosphorylation-dependent decrease corresponds to the decrease of synaptic conductance (LTD). The phosphorylation-dependent processes implicitly involve the phosphorylation-dependent changes of AMPAR conductance (Derkach et al., 1999; Banke et al., 2000). The description of kinetic constants is shown in **Figure SI5** and **Table SIl**.

**Table SIa.** Geometry of a Spine

| | $V_X$ ($\mu m^3$) | $S_X$ ($\mu m^2$) | SVR ($\mu m^{-1}$) |
|---|---|---|---|
| PSD compartment | 0.02 | 0.3585 | 17.927 |
| Cytosol compartment | 0.08 | 0.8341 | 10.425 |
| Total | 0.1 | 1.1926 | 11.926 |

**Table SIb.** Diffusion Coefficients

| | $Ca^{2+}$ | cAMP (ATP) | CaM | CaMKII | PKA |
|---|---|---|---|---|---|
| $M_x$ (kDa) | 0.04 | 0.329 (Woolf and Greer, 1994) | 16.8 (Bradshaw et al., 2002) | 649 (Bradshaw et al., 2002) | 40.5 (Woolf and Greer, 1994) |
| $D_x$ ($\mu m^2 s^{-1}$) | 600 (Stuart et al., 1999) | 500 (Stuart et al., 1999) | 250 (Luby-Phelps et al., 1995) | 6 (Woolf and Greer, 1994; Stuart et al., 1999) ††† | 32 (Woolf and Greer, 1994; Stuart et al., 1999) |

| | AC1/8 | CaN | I-1 | PP1 | PP2A | PDE |
|---|---|---|---|---|---|---|
| $M_x$ (kDa) | | 77 (Winder and Sweatt, 2001) | 28 (Winder and Sweatt, 2001) | 37 (Winder and Sweatt, 2001) | 156 (Winder and Sweatt, 2001) | 120 (Woolf and Greer, 1994) |
| $D_x$ ($\mu m^2 s^{-1}$) | 0* | 20 (Woolf and Greer, 1994) | 35.9† | 31.4†, †† | 0** | 7.2 (Woolf and Greer, 1994) |

(*) AC1/8 is a transmembrane protein.

(**) PP2A was assumed to be exclusively localized at cytosol, but not at PSD (Strack et al., 1997; Lisman and Zhabotinsky, 2001).

(†) $D_x$ were calculated from $D_x = 152 M_x^{-1/3} - 14.2$ as a relation between $M_x$ and $D_x$ (Woolf and Greer, 1994).

(††) PP1 is trapped and co-localized at PSD; therefore, $D_{PP1}$ for PSD → cytosol were assumed to take the six times smaller value (Strack et al., 1997; Bordelon et al., 2005).

(†††) Active CaMKII is trapped and co-localized at PSD; therefore, $D_{CaMKII}$ for PSD → cytosol in CaM-bound and/or phosphorylated CaMKII were assumed to take the 10 times smaller value (Strack et al., 1997; Shen et al., 2000).

**Table SIc.** Molecular Concentrations

| Molecule | Concentration (μM) | Notes |
|---|---|---|
| $Ca^{2+}$ | 0.05 | Basal $Ca^{2+}$ concentration ranges from 0.05 μM to 0.1 μM (Sabatini et al., 2002). |
| CaM | 80 | (Holmes, 2000). |
| CaMKII | 20 | CaMKII is highly abundant in PSD, where it constitutes 1-2% of the total protein (Lisman et al., 2002), and the concentration is predicted to be up to 50 μM (Erondu and Kennedy, 1985; Bradshaw et al., 2002; Petersen et al., 2003). |
| CaN | 3 | CaN is localized at PSD (Halpain et al., 1998; Gomez et al., 2002). |
| AC1/8 | 2 | Electron microscopy has revealed that AC1 is highly co-localized at PSD with weak diffusion in the spine head (Mons and Cooper, 1995; Mons et al., 1995; Wang et al., 2002). |
| ATP | 10000 | (Bhalla and Iyengar, 1999). |
| cAMP | 0.1 | Basal cAMP concentration is about 0.1 μM (Alberts et al., 2002). |
| 5'-AMP | 1000 | (Bhalla and Iyengar, 1999). |
| PDE | 1 (Buffered) | Assumption. |
| PKA | 2 (R2C2 complex), 0.05 (Free C) | PKA is highly co-localized at PSD by an anchor protein, AKAP (Carr et al., 1992; Colledge et al., 2000). |
| I-1 | 4 | Assumption. |
| PP1 | 2 | PP1 is trapped and co-localized at PSD (Strack et al., 1997; Bordelon et al., 2005). |
| PP2A | 0.03 | PP2A concentration is set lower than PP1 (Peng et al., 2004). |

**Table SId.** Molecular-Molecular Interactions in $Ca^{2+}$·CaM·CaMKII System

| No. | Kf | Kb | Notes |
|---|---|---|---|

| | | | |
|---|---|---|---|
| 1 | 51.2 $\mu M^{-1}s^{-1}$ | 200 $s^{-1}$ | (Linse et al., 1991; Brown et al., 1997; Holmes, 2000; Gaertner et al., 2004). |
| 2 | 133.3 $\mu M^{-1}s^{-1}$ | 1000 $s^{-1}$ | (Linse et al., 1991; Brown et al., 1997; Holmes, 2000; Gaertner et al., 2004). |
| 3 | 25.6 $\mu M^{-1}s^{-1}$ | 400 $s^{-1}$ | (Linse et al., 1991; Brown et al., 1997; Holmes, 2000; Gaertner et al., 2004). |
| 4 | 0.0004 $\mu M^{-1}s^{-1}$ | 1 $s^{-1}$ | (Bayer et al., 2001; Dupont et al., 2003). |
| 5 | 8 $\mu M^{-1}s^{-1}$ | 1 $s^{-1}$ | (Bradshaw et al., 2003; Dupont et al., 2003) |
| 6 | 25.6 $\mu M^{-1}s^{-1}$ | 0.02 $s^{-1}$ | (Bayer et al., 2001; Dupont et al., 2003). |
| 7 | *func* ($s^{-1}$) | 0 | *func* = 0.29 ($-0.220$ [CaMKII] + 1.826 $[CaMKII]^2$ $-$ 0.800 $[CaMKII]^3$) $\times$ [CaMKII] , where [CaMKII] = $[_{active}CaMKII]$ / [total CaMKII conc] (Dupont et al., 2003). |
| 8 | 1 $\mu M^{-1}s^{-1}$ | 1 $s^{-1}$ | (Dupont et al., 2003). |
| 9 | 8 $\mu M^{-1}s^{-1}$ | 0.001 $s^{-1}$ | (Dupont et al., 2003). |

**Table SIe.** Enzymatic Reactions in $Ca^{2+}$·CaM·CaMKII System

| No. | Km ($\mu M$) | Kcat ($s^{-1}$) | Notes |
|---|---|---|---|
| 10 | 11 | 0.335 | (Bradshaw et al., 2002; Bradshaw et al., 2003) |
| 11 | 11 | 0.335 | Assumption. |

**Table SIf.** Molecular-Molecular Interactions in AC1·cAMP·PKA System

| No. | Kf | Kb | Notes |
|---|---|---|---|
| 1 | 5 $\mu M^{-1}s^{-1}$ | 1 $s^{-1}$ | (Taylor et al., 1990; Guillou et al., 1999; Cooper, 2003; Nguyen and Woo, 2003). |
| 2 | $4\times10^{-7}$ $s^{-1}$ | 0 | Representation of basal AC activity (Guillou et al., 1999; Cooper, 2003). |
| 3 | 0.2 $\mu M^{-1}s^{-1}$ | 0.1 $s^{-1}$ | Cyclic AMP (0.5 $\mu M$) gives the half maximal kinase activity (Viste et al., 2005), and the affinity of the site A is doubly lower than that of the site B (Herberg et al., 1996), and the site B has slow binding kinetics (Taylor et al., 1990; Saucerman et al., 2003). |
| 4 | 0.1 $\mu M^{-1}s^{-1}$ | 0.2 $s^{-1}$ | (Taylor et al., 1990; Herberg et al., 1996; Saucerman et al., 2003; Viste et al., 2005). |
| 5 | 2 $\mu M^{-1}s^{-1}$ | 5 $s^{-1}$ | (Taylor et al., 1990; Herberg et al., 1996; Saucerman et al., 2003; Viste et al., 2005). |
| 6 | 4 $\mu M^{-1}s^{-1}$ | 5 $s^{-1}$ | (Taylor et al., 1990; Herberg et al., 1996; Saucerman et al., 2003; Viste et al., 2005). |

| | | | |
|---|---|---|---|
| 7 | 0.1 $\mu M^{-1}s^{-1}$ | 0.1 $s^{-1}$ | (Taylor et al., 1990; Herberg et al., 1996; Saucerman et al., 2003; Viste et al., 2005). |
| 8 | 2 $\mu M^{-1}s^{-1}$ | 10 $s^{-1}$ | (Taylor et al., 1990; Herberg et al., 1996; Saucerman et al., 2003; Viste et al., 2005). |
| 9 | 20 $\mu M^{-1}s^{-1}$ | 1 $s^{-1}$ | (Taylor et al., 1990; Herberg et al., 1996; Saucerman et al., 2003; Viste et al., 2005). |
| 10 | 200 $\mu M^{-1}s^{-1}$ | 0.1 $s^{-1}$ | (Taylor et al., 1990; Herberg et al., 1996; Saucerman et al., 2003; Viste et al., 2005). |
| 11 | 2 $s^{-1}$ | 10 $\mu M^{-1}s^{-1}$ | (Taylor et al., 1990; Herberg et al., 1996; Saucerman et al., 2003; Viste et al., 2005). |
| 12 | 20 $s^{-1}$ | 1 $\mu M^{-1}s^{-1}$ | (Taylor et al., 1990; Herberg et al., 1996; Saucerman et al., 2003; Viste et al., 2005). |
| 13 | 1 $s^{-1}$ | 20 $\mu M^{-1}s^{-1}$ | (Taylor et al., 1990; Herberg et al., 1996; Saucerman et al., 2003; Viste et al., 2005). |
| 14 | 10 $s^{-1}$ | 2 $\mu M^{-1}s^{-1}$ | (Taylor et al., 1990; Herberg et al., 1996; Saucerman et al., 2003; Viste et al., 2005). |

**Table SIg.** Enzymatic Reactions in AC1·cAMP·PKA System

| No. | Km ($\mu M$) | kcat ($s^{-1}$) | Notes |
|---|---|---|---|
| 9 | 40 | 10 | (Bhalla and Iyengar, 1999; Guillou et al., 1999; Cooper, 2003). |
| 10 | 10 | 20 | (Bhalla and Iyengar, 1999; Guillou et al., 1999; Cooper, 2003). |

**Table SIh.** Molecular-Molecular Interactions in CaN System

| No. | Kf | Kb | Notes |
|---|---|---|---|
| 1 | 40 $\mu M^{-1}s^{-1}$ | 0.04 $s^{-1}$ | The Hill coefficient of $Ca^{2+}$ -binding to CaN in the presence of excess amount of CaM is 2.5–3 (Stemmer and Klee, 1994; Klee et al., 1998). |
| 2 | 20 $\mu M^{-1}s^{-1}$ | 1 $s^{-1}$ | (Stemmer and Klee, 1994; Klee et al., 1998). |
| 3 | 10 $\mu M^{-1}s^{-1}$ | 2 $s^{-1}$ | (Stemmer and Klee, 1994; Klee et al., 1998). |

**Table SIi.** Molecular-Molecular Interactions in PP1·I-1 System

| No. | Kf ($\mu M^{-1}s^{-1}$) | Kb ($s^{-1}$) | Notes |
|---|---|---|---|
| 1 | 1 | 100 | (Huang et al., 1999; Huang and Paudel, 2000). |

**Table SIj.** Enzymatic Reactions in PP1·I-1 System

| No. | Km ($\mu M$) | kcat ($s^{-1}$) | Notes |
|---|---|---|---|
| 2 | 8.1 | 5.3 | (Hemmings et al., 1984; Huang et al., 1999; Huang |

| | | | |
|---|---|---|---|
| | | | and Paudel, 2000). |
| 3 | 3 | 2.8 | Assumption. |
| 4 | 3 | 2.8 | (Klee et al., 1998). |

**Table SIk.** Time Constants of AMPAR Recycling System

| AMPAR-State | Nophos | S845P | PDZsP | S845P/PDZsP | Notes |
|---|---|---|---|---|---|
| $K_{on}$ ($uM^{-1}$ $s^{-1}$) | 0.03 | 0.03 | 0.5 | 0.5 | AMPAR punctates exist at PSD, and AMPARs are accumulated at PSD by LTP inducing stimulation (Shi et al., 1999; Hayashi et al., 2000; Andrasfalvy and Magee, 2004). |
| $K_{off}$ ($s^{-1}$) | 0.0333 | 0.0333 | 0.0333 | 0.0333 | Mean trapping time of AMPARs by scaffold is 30–60 s (Borgdorff and Choquet, 2002). |
| $\tau_{diff}$ (s) | 0.313 | 0.313 | 0.313 | 0.313 | Calculated from 0.4 $\mu m^2 s^{-1}$ diffusion coefficient and 0.2–0.6 $\mu$m distance between PSD and cytosol (Tardin et al., 2003; Racz et al., 2004; Adesnik et al., 2005). |
| $K_{exo}$ ($s^{-1}$) | 0 | $5.55\times 10^{-4}$ | 0 | $5.55\times 10^{-4}$ | Time constant of S845-P GluR1 exocytosis is 30 min (Ehlers, 2000; Passafaro et al., 2001; Esteban et al., 2003). |
| $K_{endo}$ ($s^{-1}$) | 1 | $1.85\times 10^{-3}$ | 1 | $1.85\times 10^{-3}$ | The time constant of GluR1 endocytosis at the basal level is 9 min (Ehlers, 2000; Lin et al., 2000), and that of S845-P GluR1 was assumed to be accelerated (Kittler et al., 2005; Tigaret et al., 2006). |

**Table SII.** AMPAR Phosphorylation/Dephosphorylation

| No. | Kf ($\mu M^{-1}s^{-1}$) | Notes |
|---|---|---|
| S845 phospho by PKA | 20 | Ser845 of GluR1 is phosphorylated at the naïve state (Lee et al., 2000). Phosphorylation time constant were based on (Heynen et al., 2000; Snyder et al., 2003). |

| | | |
|---|---|---|
| PDZs phospho by CaMKII | 1 | PDZs should be dephosphorylated at the naïve state for LTP. The phosphorylation time constant was assumed to be similar to that of Ser831 of GluR1 (Lee et al., 2000). |
| S845 dephospho by PP1 and PP2A | 4 | GluR1 is phosphorylated at Ser845 in the naïve state (Lee et al., 2000). The Phosphorylation time constant was based on (Heynen et al., 2000; Snyder et al., 2003). |
| PDZs dephospho by PP1 and PP2A | 100 | PDZs should be dephosphorylated at the naïve state for LTP. The phosphorylation time constant was assumed to be similar to that of Ser831 of GluR1 (Lee et al., 2000). |
| S845 dephospho by CaN | 1.5 | GluR1 is phosphorylated at Ser845 in the naïve state (Lee et al., 2000). The phosphorylation time constant was based on (Heynen et al., 2000; Snyder et al., 2003). |
| PDZs dephospho by CaN | 1 | PDZs should be dephosphorylated at the naïve state for LTP. The phosphorylation time constant was assumed to be similar to that of Ser831 of GluR1 (Lee et al., 2000). |

## Supplemental References

Adesnik H, Nicoll RA, England PM (2005) Photoinactivation of native AMPA receptors reveals their real-time trafficking. Neuron 48:977–985.

Akyol Z, Bartos JA, Merrill MA, Faga LA, Jaren OR, Shea MA, Hell JW (2004) Apo-calmodulin binds with its C-terminal domain to the N-methyl-D-aspartate receptor NR1 C0 region. J Biol Chem 279:2166–2175.

Alberts B, Johnson A, Lewis A, Raff M, Roberts K, Wlter P (2002) Molecular biology of the cell, 4th edition. New York: Garland science.

Andrasfalvy BK, Magee JC (2004) Changes in AMPA receptor currents following LTP induction on rat CA1 pyramidal neurones. J Physiol 559:543–554.

Banke TG, Bowie D, Lee H, Huganir RL, Schousboe A, Traynelis SF (2000) Control of GluR1 AMPA receptor function by cAMP-dependent protein kinase. J Neurosci 20:89–102.

Bauman AL, Goehring AS, Scott JD (2004) Orchestration of synaptic plasticity through AKAP signaling complexes. Neuropharmacology 46:299–310.

Bayer KU, De Koninck P, Leonard AS, Hell JW, Schulman H (2001) Interaction with the NMDA receptor locks CaMKII in an active conformation. Nature 411:801–805.

Bhalla US, Iyengar R (1999) Emergent properties of networks of biological signaling pathways. Science 283:381–387.

Bi GQ, Poo MM (1998) Synaptic modifications in cultured hippocampal neurons: dependence on spike timing, synaptic strength, and postsynaptic cell type. J Neurosci 18:10464–10472.

Blanpied TA, Scott DB, Ehlers MD (2002) Dynamics and regulation of clathrin coats at specialized endocytic zones of dendrites and spines. Neuron 36:435–449.

Bordelon JR, Smith Y, Nairn AC, Colbran RJ, Greengard P, Muly EC (2005) Differential Localization of Protein Phosphatase-1$\alpha$, $\beta$ and $\gamma$1 Isoforms in Primate Prefrontal Cortex. Cereb Cortex.

Borgdorff AJ, Choquet D (2002) Regulation of AMPA receptor lateral movements. Nature 417:649–653.

Bradshaw JM, Hudmon A, Schulman H (2002) Chemical quenched flow kinetic studies indicate an intraholoenzyme autophosphorylation mechanism for $Ca^{2+}$/calmodulin-dependent protein kinase II. J Biol Chem 277:20991–20998.

Bradshaw JM, Kubota Y, Meyer T, Schulman H (2003) An ultrasensitive $Ca^{2+}$/calmodulin-dependent protein kinase II-protein phosphatase 1 switch facilitates specificity in postsynaptic calcium signaling. Proc Natl Acad Sci U S A 100:10512–10517.

Brown SE, Martin SR, Bayley PM (1997) Kinetic control of the dissociation pathway of calmodulin-peptide complexes. J Biol Chem 272:3389–3397.

Carr DW, Stofko-Hahn RE, Fraser ID, Cone RD, Scott JD (1992) Localization of the cAMP-dependent protein kinase to the postsynaptic densities by A-kinase anchoring proteins. Characterization of AKAP 79. J Biol Chem 267:16816–16823.

Carroll RC, Beattie EC, von Zastrow M, Malenka RC (2001) Role of AMPA receptor endocytosis in synaptic plasticity. Nat Rev Neurosci 2:315–324.

Castellani GC, Quinlan EM, Cooper LN, Shouval HZ (2001) A biophysical model of bidirectional synaptic plasticity: dependence on AMPA and NMDA receptors. Proc Natl Acad Sci U S A 98:12772–12777.

Chin D, Means AR (2000) Calmodulin: a prototypical calcium sensor. Trends Cell Biol 10:322–328.

Clements JD (1996) Transmitter timecourse in the synaptic cleft: its role in central synaptic function. Trends Neurosci 19:163–171.

Colledge M, Dean RA, Scott GK, Langeberg LK, Huganir RL, Scott JD (2000) Targeting of PKA to glutamate receptors through a MAGUK-AKAP complex. Neuron 27:107–119.

Collingridge GL, Isaac JT, Wang YT (2004) Receptor trafficking and synaptic plasticity. Nat Rev Neurosci 5:952–962.

Cooper DM (2003) Regulation and organization of adenylyl cyclases and cAMP. Biochem J 375:517–529.

Cousin MA, Robinson PJ (2001) The dephosphins: dephosphorylation by calcineurin

triggers synaptic vesicle endocytosis. Trends Neurosci 24:659–665.

De Koninck P, Schulman H (1998) Sensitivity of CaM kinase II to the frequency of $Ca^{2+}$ oscillations. Science 279:227–230.

Derkach V, Barria A, Soderling TR (1999) $Ca^{2+}$/calmodulin-kinase II enhances channel conductance of alpha-amino-3-hydroxy-5-methyl-4-isoxazolepropionate type glutamate receptors. Proc Natl Acad Sci U S A 96:3269–3274.

Doi T, Kuroda S, Michikawa T, Kawato M (2005) Inositol 1,4,5-trisphosphate-dependent $Ca^{2+}$ threshold dynamics detect spike timing in cerebellar Purkinje cells. J Neurosci 25:950–961.

Dupont G, Houart G, De Koninck P (2003) Sensitivity of CaM kinase II to the frequency of $Ca^{2+}$ oscillations: a simple model. Cell Calcium 34:485–497.

Ehlers MD (2000) Reinsertion or degradation of AMPA receptors determined by activity-dependent endocytic sorting. Neuron 28:511–525.

Ehlers MD, Zhang S, Bernhadt JP, Huganir RL (1996) Inactivation of NMDA receptors by direct interaction of calmodulin with the NR1 subunit. Cell 84:745–755.

Erondu NE, Kennedy MB (1985) Regional distribution of type II $Ca^{2+}$/calmodulin-dependent protein kinase in rat brain. J Neurosci 5:3270–3277.

Esteban JA, Shi SH, Wilson C, Nuriya M, Huganir RL, Malinow R (2003) PKA phosphorylation of AMPA receptor subunits controls synaptic trafficking underlying plasticity. Nat Neurosci 6:136–143.

Feng B, Stemmer PM (2001) $Ca^{2+}$ binding site 2 in calcineurin-B modulates calmodulin-dependent calcineurin phosphatase activity. Biochemistry 40:8808–8814.

Froemke RC, Dan Y (2002) Spike-timing-dependent synaptic modification induced by natural spike trains. Nature 416:433–438.

Froemke RC, Poo MM, Dan Y (2005) Spike-timing-dependent synaptic plasticity depends on dendritic location. Nature 434:221–225.

Froemke RC, Tsay IA, Raad M, Long JD, Dan Y (2006) Contribution of individual spikes in burst-induced long-term synaptic modification. J Neurophysiol

95:1620–1629.

Fukunaga K, Stoppini L, Miyamoto E, Muller D (1993) Long-term potentiation is associated with an increased activity of $Ca^{2+}$/calmodulin-dependent protein kinase II. J Biol Chem 268:7863–7867.

Gaertner TR, Putkey JA, Waxham MN (2004) RC3/Neurogranin and $Ca^{2+}$/calmodulin-dependent protein kinase II produce opposing effects on the affinity of calmodulin for calcium. J Biol Chem 279:39374–39382.

Gallagher SC, Gao ZH, Li S, Dyer RB, Trewhella J, Klee CB (2001) There is communication between all four $Ca^{2+}$-bindings sites of calcineurin B. Biochemistry 40:12094–12102.

Golding NL, Kath WL, Spruston N (2001) Dichotomy of action-potential backpropagation in CA1 pyramidal neuron dendrites. J Neurophysiol 86:2998–3010.

Golding NL, Jung HY, Mickus T, Spruston N (1999) Dendritic calcium spike initiation and repolarization are controlled by distinct potassium channel subtypes in CA1 pyramidal neurons. J Neurosci 19:8789–8798.

Gomez LL, Alam S, Smith KE, Horne E, Dell'Acqua ML (2002) Regulation of A-kinase anchoring protein 79/150-cAMP-dependent protein kinase postsynaptic targeting by NMDA receptor activation of calcineurin and remodeling of dendritic actin. J Neurosci 22:7027–7044.

Groth RD, Dunbar RL, Mermelstein PG (2003) Calcineurin regulation of neuronal plasticity. Biochem Biophys Res Commun 311:1159–1171.

Guillou JL, Nakata H, Cooper DM (1999) Inhibition by calcium of mammalian adenylyl cyclases. J Biol Chem 274:35539–35545.

Halpain S, Hipolito A, Saffer L (1998) Regulation of F-actin stability in dendritic spines by glutamate receptors and calcineurin. J Neurosci 18:9835–9844.

Hayashi Y, Shi SH, Esteban JA, Piccini A, Poncer JC, Malinow R (2000) Driving AMPA receptors into synapses by LTP and CaMKII: requirement for GluR1 and PDZ domain interaction. Science 287:2262–2267.

Hemmings HC, Jr., Nairn AC, Greengard P (1984) DARPP-32, a dopamine- and

adenosine 3':5'-monophosphate-regulated neuronal phosphoprotein. II. Comparison of the kinetics of phosphorylation of DARPP-32 and phosphatase inhibitor 1. J Biol Chem 259:14491–14497.

Herberg FW, Taylor SS, Dostmann WR (1996) Active site mutations define the pathway for the cooperative activation of cAMP-dependent protein kinase. Biochemistry 35:2934–2942.

Heynen AJ, Quinlan EM, Bae DC, Bear MF (2000) Bidirectional, activity-dependent regulation of glutamate receptors in the adult hippocampus in vivo. Neuron 28:527–536.

Hoffman DA, Magee JC, Colbert CM, Johnston D (1997) $K^+$ channel regulation of signal propagation in dendrites of hippocampal pyramidal neurons. Nature 387:869–875.

Holmes WR (2000) Models of calmodulin trapping and CaM kinase II activation in a dendritic spine. J Comput Neurosci 8:65–85.

Huang HB, Horiuchi A, Watanabe T, Shih SR, Tsay HJ, Li HC, Greengard P, Nairn AC (1999) Characterization of the inhibition of protein phosphatase-1 by DARPP-32 and inhibitor-2. J Biol Chem 274:7870–7878.

Huang KX, Paudel HK (2000) Ser67-phosphorylated inhibitor 1 is a potent protein phosphatase 1 inhibitor. Proc Natl Acad Sci U S A 97:5824–5829.

Hubbard MJ, Klee CB (1987) Calmodulin binding by calcineurin. Ligand-induced renaturation of protein immobilized on nitrocellulose. J Biol Chem 262:15062–15070.

James P, Vorherr T, Carafoli E (1995) Calmodulin-binding domains: just two faced or multi-faceted? Trends Biochem Sci 20:38–42.

Kakalis LT, Kennedy M, Sikkink R, Rusnak F, Armitage IM (1995) Characterization of the calcium-binding sites of calcineurin B. FEBS Lett 362:55–58.

Kawaguchi SY, Hirano T (2002) Signaling cascade regulating long-term potentiation of GABA(A) receptor responsiveness in cerebellar Purkinje neurons. J Neurosci 22:3969–3976.

Kim E, Sheng M (2004) PDZ domain proteins of synapses. Nat Rev Neurosci

5:771–781.

Kittler JT, Chen G, Honing S, Bogdanov Y, McAinsh K, Arancibia-Carcamo IL, Jovanovic JN, Pangalos MN, Haucke V, Yan Z, Moss SJ (2005) Phospho-dependent binding of the clathrin AP2 adaptor complex to GABAA receptors regulates the efficacy of inhibitory synaptic transmission. Proc Natl Acad Sci U S A 102:14871–14876.

Klee CB, Ren H, Wang X (1998) Regulation of the calmodulin-stimulated protein phosphatase, calcineurin. J Biol Chem 273:13367–13370.

Kuroda S, Schweighofer N, Kawato M (2001) Exploration of signal transduction pathways in cerebellar long-term depression by kinetic simulation. J Neurosci 21:5693–5702.

Lee HK, Barbarosie M, Kameyama K, Bear MF, Huganir RL (2000) Regulation of distinct AMPA receptor phosphorylation sites during bidirectional synaptic plasticity. Nature 405:955–959.

Leonard AS, Bayer KU, Merrill MA, Lim IA, Shea MA, Schulman H, Hell JW (2002) Regulation of calcium/calmodulin-dependent protein kinase II docking to N-methyl-D-aspartate receptors by calcium/calmodulin and $\alpha$-actinin. J Biol Chem 277:48441–48448.

Lin JW, Ju W, Foster K, Lee SH, Ahmadian G, Wyszynski M, Wang YT, Sheng M (2000) Distinct molecular mechanisms and divergent endocytotic pathways of AMPA receptor internalization. Nat Neurosci 3:1282–1290.

Linse S, Helmersson A, Forsen S (1991) Calcium binding to calmodulin and its globular domains. J Biol Chem 266:8050–8054.

Lisman J, Schulman H, Cline H (2002) The molecular basis of CaMKII function in synaptic and behavioural memory. Nat Rev Neurosci 3:175–190.

Lisman JE, Zhabotinsky AM (2001) A model of synaptic memory: a CaMKII/PP1 switch that potentiates transmission by organizing an AMPA receptor anchoring assembly. Neuron 31:191–201.

Luby-Phelps K, Hori M, Phelps JM, Won D (1995) $Ca^{2+}$-regulated dynamic

compartmentalization of calmodulin in living smooth muscle cells. J Biol Chem 270:21532–21538.

Malinow R, Malenka RC (2002) AMPA receptor trafficking and synaptic plasticity. Annu Rev Neurosci 25:103–126.

Matveev V, Wang XJ (2000) Implications of all-or-none synaptic transmission and short-term depression beyond vesicle depletion: a computational study. J Neurosci 20:1575–1588.

Mauceri D, Cattabeni F, Di Luca M, Gardoni F (2004) Calcium/calmodulin-dependent protein kinase II phosphorylation drives synapse-associated protein 97 into spines. J Biol Chem 279:23813–23821.

Meng Y, Zhang Y, Jia Z (2003) Synaptic transmission and plasticity in the absence of AMPA glutamate receptor GluR2 and GluR3. Neuron 39:163–176.

Migliore M (1996) Modeling the attenuation and failure of action potentials in the dendrites of hippocampal neurons. Biophys J 71:2394–2403.

Migliore M, Hoffman DA, Magee JC, Johnston D (1999) Role of an A-type $K^+$ conductance in the back-propagation of action potentials in the dendrites of hippocampal pyramidal neurons. J Comput Neurosci 7:5–15.

Mons N, Cooper DM (1995) Adenylate cyclases: critical foci in neuronal signaling. Trends Neurosci 18:536–542.

Mons N, Harry A, Dubourg P, Premont RT, Iyengar R, Cooper DM (1995) Immunohistochemical localization of adenylyl cyclase in rat brain indicates a highly selective concentration at synapses. Proc Natl Acad Sci U S A 92:8473–8477.

Neville KR, Lytton WW (1999) Potentiation of $Ca^{2+}$ influx through NMDA channels by action potentials: a computer model. Neuroreport 10:3711–3716.

Nguyen PV, Woo NH (2003) Regulation of hippocampal synaptic plasticity by cyclic AMP-dependent protein kinases. Prog Neurobiol 71:401–437.

Passafaro M, Piech V, Sheng M (2001) Subunit-specific temporal and spatial patterns of AMPA receptor exocytosis in hippocampal neurons. Nat Neurosci 4:917–926.

Peng J, Kim MJ, Cheng D, Duong DM, Gygi SP, Sheng M (2004) Semiquantitative proteomic analysis of rat forebrain postsynaptic density fractions by mass spectrometry. J Biol Chem 279:21003–21011.

Petersen JD, Chen X, Vinade L, Dosemeci A, Lisman JE, Reese TS (2003) Distribution of postsynaptic density (PSD)-95 and $Ca^{2+}$/calmodulin-dependent protein kinase II at the PSD. J Neurosci 23:11270–11278.

Poirazi P, Brannon T, Mel BW (2003) Arithmetic of subthreshold synaptic summation in a model CA1 pyramidal cell. Neuron 37:977–987.

Price NE, Mumby MC (1999) Brain protein serine/threonine phosphatases. Curr Opin Neurobiol 9:336–342.

Racz B, Blanpied TA, Ehlers MD, Weinberg RJ (2004) Lateral organization of endocytic machinery in dendritic spines. Nat Neurosci 7:917–918.

Rycroft BK, Gibb AJ (2002) Direct effects of calmodulin on NMDA receptor single-channel gating in rat hippocampal granule cells. J Neurosci 22:8860–8868.

Sabatini BL, Maravall M, Svoboda K (2001) $Ca^{2+}$ signaling in dendritic spines. Curr Opin Neurobiol 11:349–356.

Sabatini BL, Oertner TG, Svoboda K (2002) The life cycle of $Ca^{2+}$ ions in dendritic spines. Neuron 33:439–452.

Sans N, Racca C, Petralia RS, Wang YX, McCallum J, Wenthold RJ (2001) Synapse-associated protein 97 selectively associates with a subset of AMPA receptors early in their biosynthetic pathway. J Neurosci 21:7506–7516.

Sasagawa S, Ozaki Y, Fujita K, Kuroda S (2005) Prediction and validation of the distinct dynamics of transient and sustained ERK activation. Nat Cell Biol 7:365–373.

Saucerman JJ, Brunton LL, Michailova AP, McCulloch AD (2003) Modeling β-adrenergic control of cardiac myocyte contractility in silico. J Biol Chem 278:47997–48003.

Shen K, Teruel MN, Connor JH, Shenolikar S, Meyer T (2000) Molecular memory by reversible translocation of calcium/calmodulin-dependent protein kinase II. Nat Neurosci 3:881–886.

Shi SH, Hayashi Y, Petralia RS, Zaman SH, Wenthold RJ, Svoboda K, Malinow R (1999) Rapid spine delivery and redistribution of AMPA receptors after synaptic NMDA receptor activation. Science 284:1811–1816.

Snyder GL, Galdi S, Fienberg AA, Allen P, Nairn AC, Greengard P (2003) Regulation of AMPA receptor dephosphorylation by glutamate receptor agonists. Neuropharmacology 45:703–713.

Stemmer PM, Klee CB (1994) Dual calcium ion regulation of calcineurin by calmodulin and calcineurin B. Biochemistry 33:6859–6866.

Strack S, Choi S, Lovinger DM, Colbran RJ (1997) Translocation of autophosphorylated calcium/calmodulin-dependent protein kinase II to the postsynaptic density. J Biol Chem 272:13467–13470.

Stuart G, Spruston N, Hausser M, eds (1999) Dendrites: Oxford University Press.

Tardin C, Cognet L, Bats C, Lounis B, Choquet D (2003) Direct imaging of lateral movements of AMPA receptors inside synapses. EMBO J 22:4656–4665.

Taylor SS, Buechler JA, Yonemoto W (1990) cAMP-dependent protein kinase: framework for a diverse family of regulatory enzymes. Annu Rev Biochem 59:971–1005.

Tigaret CM, Thalhammer A, Rast GF, Specht CG, Auberson YP, Stewart MG, Schoepfer R (2006) Subunit dependencies of N-methyl-D-aspartate (NMDA) receptor-induced $\alpha$-amino-3-hydroxy-5-methyl-4-isoxazolepropionic acid (AMPA) receptor internalization. Mol Pharmacol 69:1251–1259.

Tomita S, Stein V, Stocker TJ, Nicoll RA, Bredt DS (2005) Bidirectional synaptic plasticity regulated by phosphorylation of stargazin-like TARPs. Neuron 45:269–277.

Triller A, Choquet D (2005) Surface trafficking of receptors between synaptic and extrasynaptic membranes: and yet they do move! Trends Neurosci 28:133–139.

Tsodyks MV, Markram H (1997) The neural code between neocortical pyramidal neurons depends on neurotransmitter release probability. Proc Natl Acad Sci U S A 94:719–723.

Vandenberghe W, Nicoll RA, Bredt DS (2005) Stargazin is an AMPA receptor auxiliary

subunit. Proc Natl Acad Sci U S A 102:485–490.

Viste K, Kopperud RK, Christensen AE, Doskeland SO (2005) Substrate enhances the sensitivity of type I protein kinase a to cAMP. J Biol Chem 280:13279–13284.

Wang H, Chan GC, Athos J, Storm DR (2002) Synaptic concentration of type-I adenylyl cyclase in cerebellar neurons. J Neurochem 83:946–954.

Winder DG, Sweatt JD (2001) Roles of serine/threonine phosphatases in hippocampal synaptic plasticity. Nat Rev Neurosci 2:461–474.

Woolf TB, Greer CA (1994) Local communication within dendritic spines: Models of second messenger diffusion in granule cell spines of the mammalian olfactory bulb. Synapse 17:247–267.

Xia Z, Storm DR (1997) Calmodulin-regulated adenylyl cyclases and neuromodulation. Curr Opin Neurobiol 7:391–396.